

Heatwave Events over the Yangtze River Basin

Subjects: [Meteorology & Atmospheric Sciences](#)

Contributor: Zhibo Gao

Heatwave events (HWEs) have strong impacts on human health, ecosystems, and sustainable social development. In the future, the increase in HWEs over the Yangtze River Basin (YRB) region is likely to be associated with the enhancement of the western-Pacific subtropical high (WPSH) and South-Asian high (SAH), and this enhancement was also greater under SSP585. The results from the high-resolution simulation of the RCM can provide an important reference for disaster prevention and mitigation in the future.

WRF model

projection

Yangtze River Basin

1. Introduction

Reliable weather and climate forecasts of Heatwave events (HWEs) are essential for risk mitigation and early-warning systems ^[1]. Most global climate models (GCMs), with resolutions from 100 km to 200 km, are generally good in capturing large-scale circulation ^{[2][3][4]}, but they are not efficient enough to represent the fine-scale processes of the atmosphere, as well as the terrain and land-use distribution, which makes it difficult to accurately characterize regional HWEs ^{[5][6][7][8]}. Regional climate models (RCMs), with refined grid spacing and solid-model physics, can address the abovementioned problems associated with GCMs very well ^{[9][10][11]}. Several studies have indicated that RCMs are believed to provide more added value in their simulations with respect to GCMs ^{[12][13][14][15]}. Based on the above facts, it is important and meaningful to use RCMs to study the mechanisms and variation of HWEs in a certain area ^{[16][17][18]}.

The Yangtze River Basin (YRB) is one of the core regions for the occurrence of HWEs in China ^[19]. A large number of studies have focused on how HWEs in this region are generated from the perspective of large-scale circulation anomalies ^{[19][20]}, variability in the sea-surface temperature (SST) ^[21], and anomalous boundary characteristics in observational diagnostics ^[22]. Li, Xiao, and Zhao ^[20] suggested that the occurrence of HWEs is strongly associated with the joint effects of the western-Pacific subtropical high (WPSH) and the South-Asian high (SAH). In addition, Teng and Branstator ^[23] pointed out that the East-Asian jet stream (EAJS) can act as a waveguide to adjust the intensity and position of the WPSH through quasi-zonal teleconnections, which further influence the HWEs in the YRB region. It is also indicated that the strong SST anomaly over the mid-North Atlantic connects to the WPSH and East-Asian upper-level westerlies via the teleconnection wave train and can further contribute to the variability of HWEs over the YRB region ^[24].

2. Characteristics of HWEs in the Historical Period

The summer mean Tmax over the YRB increased slowly, and it exhibited an obvious interdecadal shift at approximately 2000, which became a positive anomaly (**Figure 1a**). Correspondingly, the total number of HWEs also showed a slow rise and shifts in 2000 (**Figure 1b**). It is also worth mentioning that the YRB experienced persistent HWEs in 2013, and the Tmax of many weather stations set a new record. Interestingly, although the total number of HWEs is increasing; the short-lived HWEs have not risen so much, except for more occurrences in approximately 2005; and there was no obvious upward trend in other years (**Figure 1c**). However, it should be mentioned that the number of long-lived HWEs increased obviously during the study period, which is the main reason for the increase in the total number of HWEs (**Figure 1d**). Similar characteristics can be found for the variation in HWDs between the two classes of HWEs (**Figure 1e,f**). Therefore, HWEs with long durations were the main type of HWEs from 1981 to 2018, and they dominated the increase in total HWEs in the YRB region.

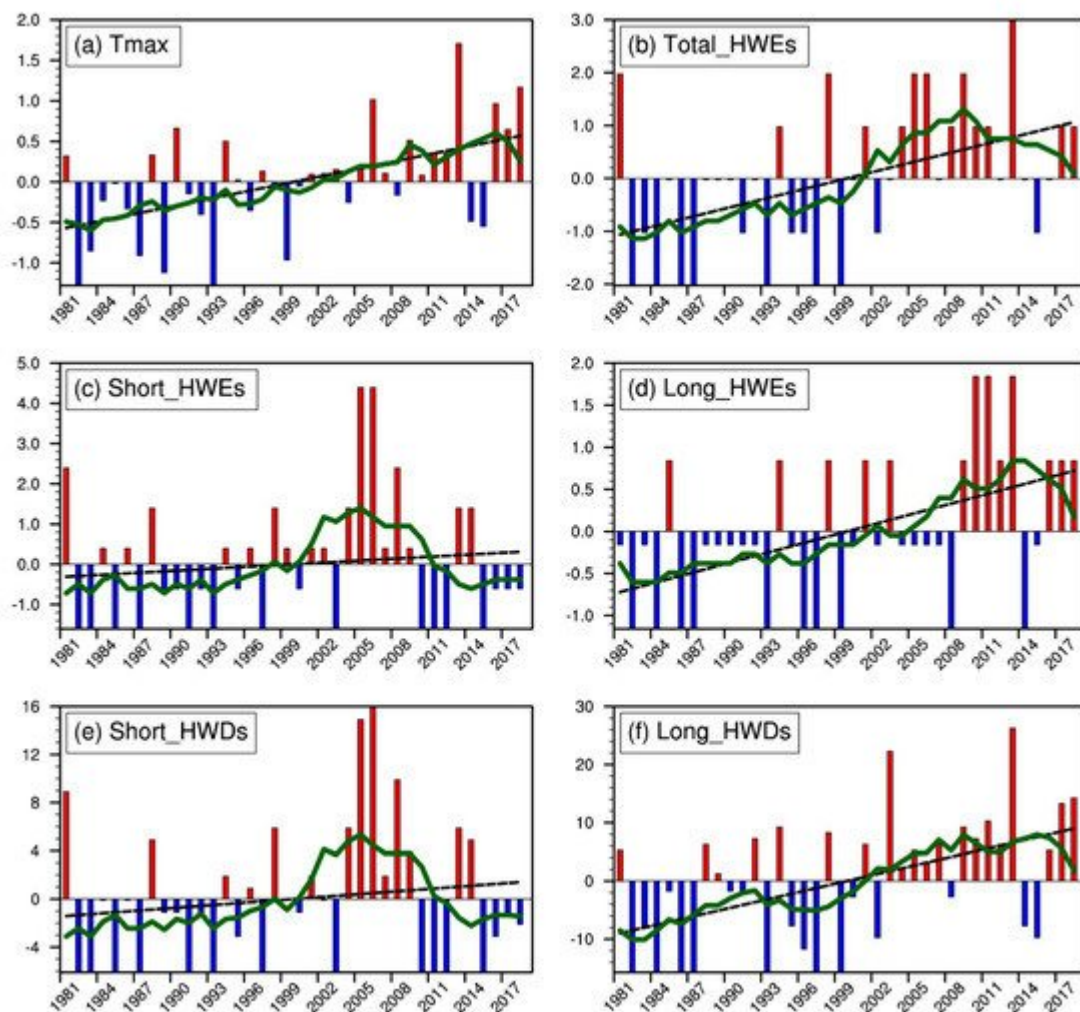


Figure 1. (a) Anomalies of mean daily maximum temperature at 2 m (°C) and anomalies in the number of (b) total HWEs (events), (c) short-lived HWEs (events), (d) long-lived HWEs (events), (e) short-lived HWDs (days), and (f) long-lived HWDs (days) during summer over the YRB region. The black dashed lines denote the linear trends, and the green solid lines represent the nine-year running average.

3. Projection of HWEs

Before using the RCM to make projections of HWEs in the YRB region, the simulation results were first analyzed in reference periods to verify the model's ability to simulate HWEs. Because Tmax is the most important indicator for HWEs, the entry mainly focused on the prediction skill of Tmax. The model can simulate the spatial distribution of the average daily Tmax in summer very well (**Figure 2a,b**), although there is a certain cold bias in the northern YRB region. From the perspective of time evolution, the model can also simulate the interannual variation in the regional average Tmax very well (**Figure 2c**). The R between the model and observations reached 0.45, exceeding the 95% confidence level. In addition, the model also has a certain ability to simulate the number of HWDs in different years. The R reached 0.39 and passed the 90% confidence level (**Figure 2d**). Therefore, the model has a certain ability to simulate the HWEs in the YRB region, which indicates that it can be used to predict the future variation in HWEs in this region.

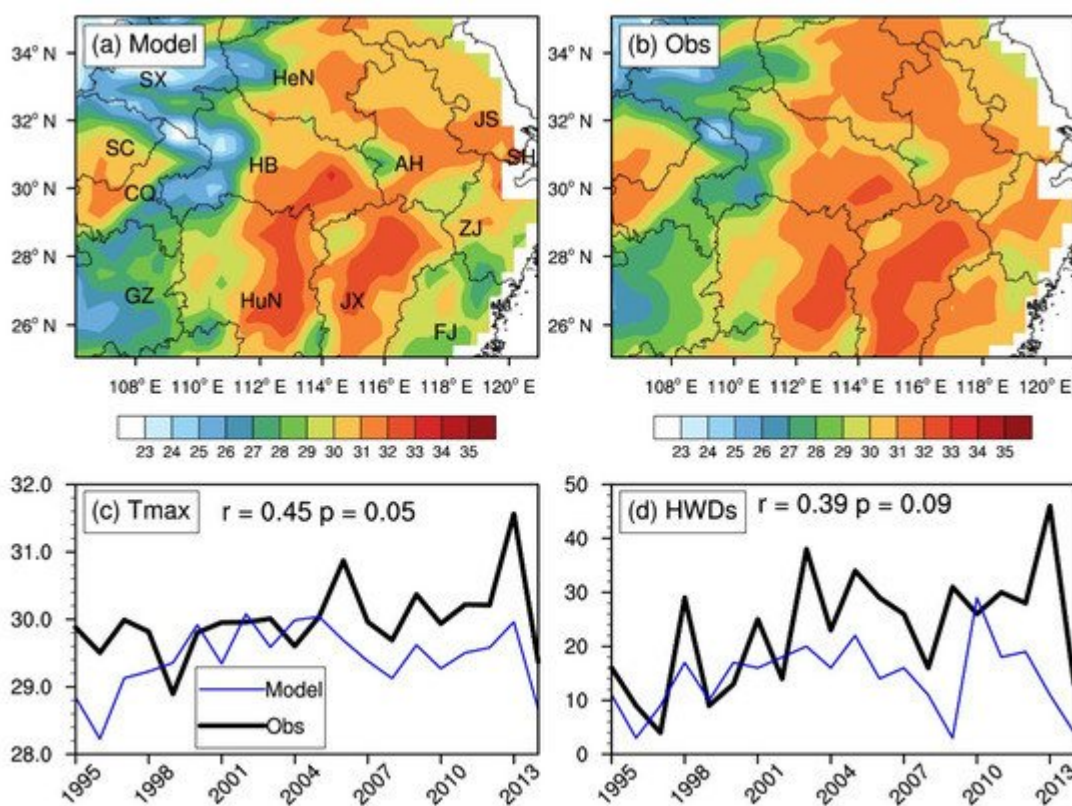


Figure 2. Spatial distributions of the average Tmax (°C) in summer from 1995 to 2014 for (a) model and (b) observation, (c) time series of the spatially averaged daily Tmax (°C) in the YRB during summer, and (d) time series of the total HWDs (days) in the YRB during summer.

In the future, the average Tmax in summer over the YRB will rise obviously (**Figure 3a**). The upward trend of SSP585 will be greater than that of SSP245. Relative to the average of 1995–2014 reference period, the temperature of SSP585 will rise by more than 1.8 °C in the middle of the century. The total number of HWEs will also rise under the impact of increasing temperatures, especially in the SSP585 scenario, which will increase by 1.8 events per year by mid-century (**Figure 3b**). It should be mentioned that there is a great difference in the changes of the short-lived HWEs under the two scenarios (**Figure 3c**). For SSP245, short-lived HWEs first increase and then decrease, with a relatively flat trend. However, for SSP585, although there is also a slight

downward trend after 2024, the overall upward trend of short-lived HWEs is particularly obvious, which will increase by 1.5 events per year in the middle of the century. As for the long-lived HWEs, they will increase obviously in both future scenarios (**Figure 3d**), which may cause large challenges for future disaster prevention and mitigation work.

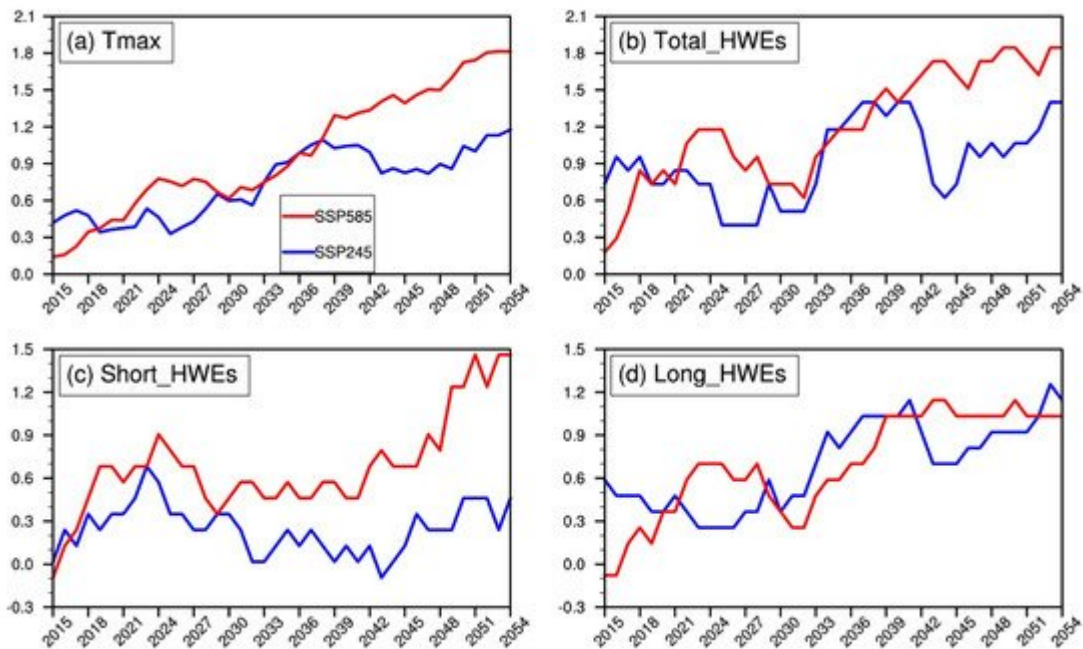


Figure 3. The anomalies in (a) Tmax ($^{\circ}\text{C}$), (b) total HWEs (events), (c) short-lived HWEs (events), and (d) long-lived HWEs (events) relative to the 1995–2014 reference period averaged over the YRB region. The time series were smoothed with a 9-year running mean filter.

4. Conclusions

In the context of global warming, HWEs are becoming increasingly frequent, and obvious differences exist between different regions. The YRB region, an important economic center of China, is one of the regions where HWEs are more frequent and severe. Coarse-resolution models (such as GCMs) cannot resolve the detailed characteristics of HWEs. Based on this, a high-resolution RCM (WRF) and observation dataset (CN051) were used to analyze the characteristics of HWEs in the historical period and project the changes in HWEs in the YRB in the future. The main findings are as follows.

1. During the 1981–2018 historical period, the Tmax, long-lived HWEs, and total HWEs in the YRB area all showed an obvious upward trend, and the turning point occurred in approximately 2000. Although the upward trend of short-lived HWEs was relatively small overall, there was a significant increase in certain regions, such as Henan, Sichuan, and the eastern coastal region. At the same time, the high incidence of long-lived HWEs was mainly concentrated in Hubei, Hunan, and eastern Sichuan provinces.
2. Through the high-resolution simulation during the reference period, it was found that the WRF model can simulate the daily Tmax very well, which provides reliability for the projections. The projection results show that

Tmax, long-lived HWEs, and total HWEs will increase obviously in both scenarios, and the upward trend of SSP585 is even greater. Short-lived HWEs will also increase under the SSP585 scenario, but they are relatively stable overall under SSP245. For SSP245, in the northern region, the daily Tmax will rise faster, and short-lived HWEs will increase, while the long-lived HWEs will rise significantly in the southern YRB. However, both short-lived and long-lived HWEs will increase in each subregion of the YRB under the SSP585 scenario.

3. In both future scenarios, the geopotential heights at 500 hPa and 200 hPa over the YRB will increase, which may imply that both the WPSH and SAH will be enhanced, and this is more pronounced in the SSP585 scenario. Changes in the WPSH and SAH have an important impact on the HWEs of the YRB. The long-lived HWEs are caused by the joint effect of the WPSH and SAH, and this joint effect will also affect the short-lived HWEs under the SSP585 scenario. As mentioned in the fourth part, the detailed physical mechanism of the impact of geopotential height on HWEs still needs further study in the future.

References

1. Yang, J.; Zhu, T.; Gao, M.; Lin, H.; Wang, B.; Bao, Q. Late-July barrier for subseasonal forecast of summer daily maximum temperature over Yangtze River Basin. *Geophys. Res. Lett.* 2018, 45, 12610–12615.
2. Torres-Alavez, J.A.; Giorgi, F.; Kucharski, F.; Coppola, E.; Castro-García, L. ENSO teleconnections in an ensemble of CORDEX-CORE regional simulations. *Clim. Dyn.* 2021, 57, 1445–1461.
3. Lin, L.; Gettelman, A.; Xu, Y.; Wu, C.; Wang, Z.; Rosenbloom, N.; Bates, S.C.; Dong, W. CAM6 simulation of mean and extreme precipitation over Asia: Sensitivity to upgraded physical parameterizations and higher horizontal resolution. *Geosci. Model Dev.* 2019, 12, 3773–3793.
4. Anand, A.; Bhowmick, M.; Mishra, S.K.; Sahany, S.; Reddy Telukuntla, C.V. Response of Indian monsoon to increase of resolution in NCAR-CAM5. *Atmos. Res.* 2019, 221, 12–26.
5. Yan, Y.; Tang, J.; Wang, S.; Niu, X.; Le, W. Uncertainty of land surface model and land use data on WRF model simulations over China. *Clim. Dyn.* 2021, 57, 1833–1851.
6. Gao, Z.; Zhu, J.; Guo, Y.; Yan, X.; Wang, X.; Li, H.; Li, S. Comparison of different land-surface perturbation methods in short-range ensemble forecasts. *Atmos. Ocean. Sci. Lett.* 2021, 14, 100045.
7. Kong, X.; Wang, A.; Bi, X.; Li, X.; Zhang, H. Effects of horizontal resolution on hourly precipitation in AGCM simulations. *J. Hydrometeorol.* 2020, 21, 643–670.
8. Liang, X.-Z.; Sun, C.; Zheng, X.; Dai, Y.; Xu, M.; Choi, H.I.; Ling, T.; Qiao, F.; Kong, X.; Bi, X.; et al. CWRf performance at downscaling China climate characteristics. *Clim. Dyn.* 2018, 52, 2159–2184.

9. Zhu, X.; Wei, Z.; Dong, W.; Ji, Z.; Wen, X.; Zheng, Z.; Yan, D.; Chen, D. Dynamical downscaling simulation and projection for mean and extreme temperature and precipitation over central Asia. *Clim. Dyn.* 2020, 54, 3279–3306.
10. Tian, L.; Jin, J.; Wu, P.; Niu, G.-y.; Zhao, C. High-resolution simulations of mean and extreme precipitation with WRF for the soil-erosive Loess Plateau. *Clim. Dyn.* 2020, 54, 3489–3506.
11. Cardoso, R.M.; Soares, P.M.M.; Miranda, P.M.A.; Belo-Pereira, M. WRF high resolution simulation of Iberian mean and extreme precipitation climate. *Int. J. Clim.* 2013, 33, 2591–2608.
12. Yun, Y.; Liu, C.; Luo, Y.; Gao, W. Warm-season mesoscale convective systems over eastern China: Convection-permitting climate model simulation and observation. *Clim. Dyn.* 2021, 57, 3599–3617.
13. Gao, Z.; Zhu, J.; Guo, Y.; Luo, N.; Fu, Y.; Wang, T. Impact of land surface processes on a record-breaking rainfall event on May 06–07, 2017, in Guangzhou, China. *J. Geophys. Res. Atmos.* 2021, 126, e2020JD032997.
14. Yun, Y.; Liu, C.; Luo, Y.; Liang, X.; Huang, L.; Chen, F.; Rasmussen, R. Convection-permitting regional climate simulation of warm-season precipitation over Eastern China. *Clim. Dyn.* 2019, 54, 1469–1489.
15. Guo, Z.; Fang, J.; Sun, X.; Yang, Y.; Tang, J. Sensitivity of summer precipitation simulation to microphysics parameterization over Eastern China: Convection-permitting regional climate simulation. *J. Geophys. Res. Atmos.* 2019, 124, 9183–9204.
16. Kong, X.; Wang, A.; Bi, X.; Wang, D. Assessment of temperature extremes in China using RegCM4 and WRF. *Adv. Atmos. Sci.* 2019, 36, 363–377.
17. Fita, L.; Polcher, J.; Giannaros, T.M.; Lorenz, T.; Milovac, J.; Sofiadis, G.; Katragkou, E.; Bastin, S. CORDEX-WRF v1.3: Development of a module for the weather research and forecasting (WRF) model to support the CORDEX community. *Geosci. Model Dev.* 2019, 12, 1029–1066.
18. Yu, E.; Sun, J.; Chen, H.; Xiang, W. Evaluation of a high-resolution historical simulation over China: Climatology and extremes. *Clim. Dyn.* 2014, 45, 2013–2031.
19. Qi, X.; Yang, J.; Gao, M.; Yang, H.; Liu, H. Roles of the tropical/extratropical intraseasonal oscillations on generating the heat wave over Yangtze River valley: A numerical study. *J. Geophys. Res. Atmos.* 2019, 124, 3110–3123.
20. Li, N.; Xiao, Z.; Zhao, L. A recent increase in long-lived heatwaves in China under the joint influence of South Asia and Western North Pacific subtropical highs. *J. Clim.* 2021, 34, 7167–7179.
21. Yang, K.; Zhang, J.; Wu, L.; Wei, J. Prediction of summer hot extremes over the middle and lower reaches of the Yangtze River valley. *Clim. Dyn.* 2018, 52, 2943–2957.

22. Gao, M.; Wang, B.; Yang, J.; Dong, W. Are peak summer sultry heat wave days over the Yangtze–Huaihe River Basin predictable? *J. Clim.* 2018, 31, 2185–2196.
23. Teng, H.; Branstator, G. Tropospheric waveguide teleconnections and their seasonality. *J. Atmos. Sci.* 2017, 74, 1513–1532.
24. Sun, J. Record-breaking SST over mid-North Atlantic and extreme high temperature over the Jianghuai–Jiangnan region of China in 2013. *Chin. Sci. Bull.* 2014, 59, 3465–3470.

Retrieved from <https://encyclopedia.pub/entry/history/show/45404>